View metadata, citation and similar papers at core.ac.uk
brought to you by CORE
provided by NASA Technical Reports Server

LaRC Aerothermodynamic Ground Tests in Support of BOLT Flight Experiment

Scott A. Berry,* Michelle L. Mason,† Frank A. Greene,* Rudy A. King,‡ and Elizabeth F. Rieken†
NASA Langley Research Center, Hampton, VA, 23681

and
Kevin D. Basore§
Universities Space Research Association, Hampton, VA 23666

A review is provided of recent aerothermodynamic ground-test contributions by NASA Langley Research Center (LaRC) to the BOLT flight test program. Several test entries into the Langley Aerothermodynamic Laboratory 20-Inch Mach 6 Air Tunnel are discussed. These entries were intended to support the development and design of flight hardware and instrumentation. Some trends and observations from these entries are provided. Also, a comparison of two different global heat transfer test techniques is included and discussed.

I. Nomenclature

M	Mach number
Re	unit Reynolds number (1/ft)
x	longitudinal distance from the nose (in)
L	model reference length from nose to end of body (in)
α	model angle of attack (deg)
h	heat transfer coefficient (lbm/ft^2-sec)
h_{Ref}	reference coefficient using Fay-Riddell calculation to stagnation point of a sphere

II. Introduction

The Boundary Layer Transition (BOLT) Flight Experiment was recently initiated with John Hopkins University Applied Physics Laboratory (JHU/APL) leading a team of government, industry, and academic participants. BOLT is sponsored by the Air Force Office of Scientific Research (AFOSR) and is intended to serve as a follow-on to the Hypersonic International Flight Research Experimentation (HIFiRE) series of flight experiments. With increasing geometric complexity, each boundary layer transition flight has sought to build upon the success of the former, first starting with HIFiRE 1 on a straight cone, then HIFiRE 5 on an elliptic cone, and now BOLT, a three-dimensional body with concave surfaces and swept leading edges. The main objective of BOLT is to use the latest state-of-the-art numerical transition prediction tools, combined with ground-test data, to design, build, and fly on a sounding rocket a high-quality boundary layer experiment at hypersonic conditions. Reference 1 provides an overview of BOLT, while Ref. 2 discusses some recent ground-testing initiated in support of the flight experiment.

The BOLT effort was officially established in September 2017 with the selection of JHU/APL as the lead for design and development of the flight vehicle, along with the announcement of the open competition to select a launch services provider. At the kick-off meeting, NASA Langley Research Center (LaRC) provided to the project an initial set of aeroheating data based on the preliminary version of the BOLT geometry. Utilizing LaRC's phosphor thermography technique, data were obtained in less than three weeks after getting the geometry from the government team that was leading the selection process and early design. A multiple view sketch of the basic geometry is provided in Fig. 1. Note, the top and bottom surfaces in the lower left image of Fig. 1 are the primary surfaces of interest; the highly curved regions in between are referred to as the gutters.

* Research Engineer, Aerothermodynamics Branch, M/S 408A, Associate Fellow AIAA.
† Research Engineer, Aerothermodynamics Branch, M/S 408A, Member AIAA.
‡ Research Engineer, Flow Physics & Control Branch, M/S 170, Member AIAA.
§ Former NIFS Intern; Now, Systems Engineer, Raytheon Missile Systems, 9000 S Rita Rd, Tucson, AZ, Member AIAA.

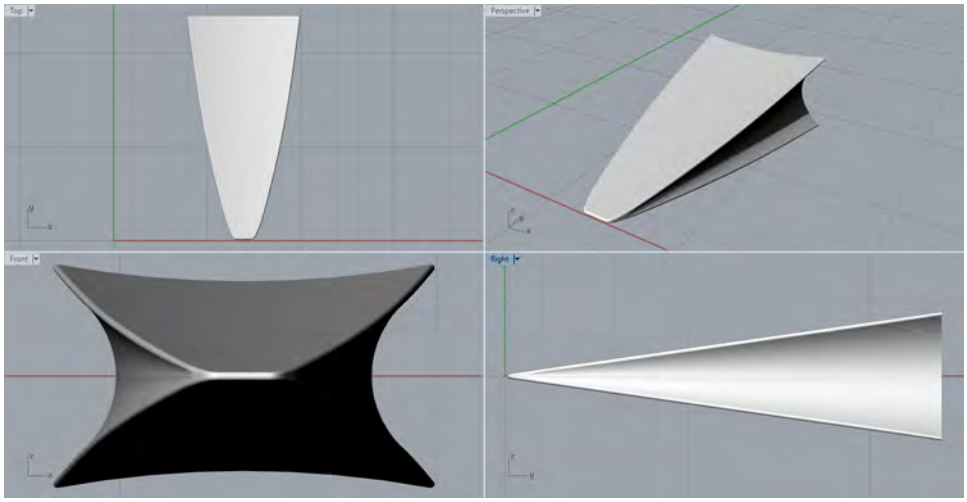

Figure 1. Multiview sketch showing basic BOLT geometry.

The BOLT project has been progressing through the first year of a three year effort, focused thus far on the design of the flight vehicle based on the extensive experimental and computational results to date. The second year will switch to an emphasis on building the hardware, while the final year will revolve around the flight test and subsequent detailed analysis. The launch provider has now been selected as the German Aerospace Center (DLR) Mobile Rocket Base (MORABA), which has been the same provider for many of the HIFiRE flights. The launch is presently set for Q2 of CY20 at Esrange, Sweden. While this paper is primarily intended to provide an overview of LaRC contributions to the BOLT project, it also serves to compare and contrast results from different test techniques for obtaining global heat transfer results.

III. Experimental Method

A. Test Facility

The present experimental results were obtained in the LaRC 20-Inch Mach 6 Air Tunnel. Berger, et al.[3] provides details of this hypersonic blowdown facility, which uses heated, dried, and filtered air as the test gas. Typical operating conditions for the tunnel are stagnation pressures ranging from 30 to 500 psia, stagnation temperatures from 760 to 940 degR, and freestream unit Reynolds numbers from 0.5 to 8 million per foot. A two-dimensional, contoured nozzle is used to provide perfect-gas freestream conditions with freestream Mach numbers from 5.8 to 6.1. The nozzle throat is 0.34 by 20.5 in, which then expands into the 20 by 20.5 in test section. A bottom-mounted model injection system is typically used to insert models from a sheltered position to the tunnel centerline, which for these aeroheating tests was done as quickly as possible (less than 0.5 sec traverse through the tunnel boundary layer). Run times up to 20 minutes are possible with this facility, although for the current heat transfer tests, the model was exposed to the flow for only a few seconds. Flow conditions are typically determined based on perfect-gas calculations from the measured reservoir pressure and temperature and the measured pitot pressure at the test section.

B. Test Techniques

The two-color relative-intensity phosphor thermography technique is now the default test technique for aeroheating studies in LaRC's Aerothermodynamics Laboratory (LAL). Details of the phosphor thermography technique are provided in Refs. 4, 5, and 6. References 7, 8, and 9 are examples of the application of this technique to wind tunnel testing. The primary advantage of phosphor thermography is the global resolution of the quantitative heat transfer data. Such data can be used to identify the heating footprint of complex, three-dimensional flow phenomena (e.g., transition fronts, turbulent wedges, boundary-layer vortices, etc.) that are extremely difficult to resolve by discrete measurement techniques. Quantitative global surface heating information is obtained from models that can be fabricated quickly (a few weeks) and economically (an order of magnitude less than the thin-film technique). Past comparisons of heat transfer measurements obtained from phosphor thermography to conventional thin-film measurements (Ref. 10) and CFD predictions (Ref. 11 and 12) have shown excellent agreement.

While the thermographic phosphor technique has become LaRC's standard for aeroheating studies, there is a weakness with the technique that is exposed by studies requiring small and precise surface features. The casting process and phosphor surface coating can lead to decreased fidelity of these small surface features. The phosphor coating is on the order of 0.001-in thick, so if the purpose of the study is to look at the effect of something that is on that same order, then significant discrepancies might be included in the observations. A newer test technique is under development at LaRC, whereby an infrared (IR) camera is used to monitor the surface temperatures on very accurately milled models built from a relatively cheap resin material called PEEK (poly-ether-ether-ketone). The advantage of this approach is that surface deviations are not introduced due to the casting process (i.e., model shrinkage and/or microfractures), and an overcoat is not required. The use of PEEK with IR has been reported in the literature for a few years (for instance, see Ref. 13). Thus, LaRC has taken steps recently to explore this alternate approach to aeroheating studies for cases that require stricter control of model fidelity. The current assessment of PEEK models in the LAL provides an opportunity to examine the practicality of this substrate material, and also to evaluate the quantitative aspects of the approach. In terms of practicality, three basic questions are important: (1) the expense and (2) time required to build the models, and (3) can the material withstand LAL conditions? For quantitative results, there is the obvious need for well-known thermal and optical properties of the material over a wide range of surface temperatures. The IR setup for the present study consists of a FLIR SC6701 SLS longwave (7.5-9.5 micrometers) IR camera looking through a large zinc selenide window at the top of the tunnel. The camera, which provides 640x512 pixel resolution, comes with 25, 50, and 100 mm lens options. The camera framing rate was 60 Hz, with the lens, location, and view angle set to optimize the size of model in the imager, while being as close to perpendicular as possible to the model surface of interest.

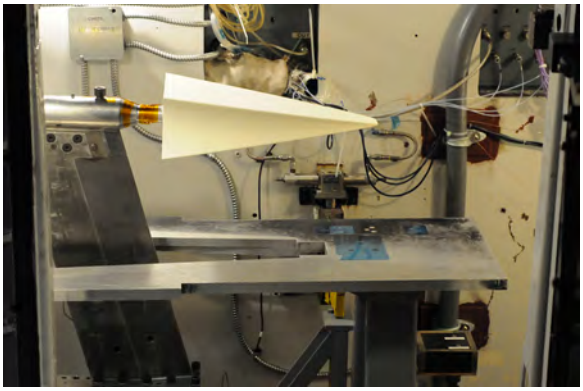

Figure 2. Half-scale BOLT phosphor thermography model shown in the 20-In Mach 6 Tunnel in the retracted position at nominal alpha and beta.

C. Models

The BOLT flight geometry is described in Ref 1 as 866 mm, or 34.1 inches long. The flight nose radius is listed as 5 mm, or 0.197 in. The initial test at Langley was with a half scale model (17-in long) using our standard phosphor thermography technique; thus, the model was built using our cast ceramic technique. Taking advantage of tunnel availability just ahead of the BOLT project kick-off, a preliminary version of the CAD geometry* was obtained from the BOLT team and used to construct and test a model in less than three weeks. Figure 2 provides a photograph of the phosphor thermography BOLT model installed in the retracted position of the Langley 20-Inch Mach 6 Air Tunnel. A second model was built by LaRC out of PEEK. This model was 12-in long, or roughly a third scale model (also using the preliminary CAD geometry) and was intended to include small regions of distributed roughness near the swept leading edges (LE). (More discussion on the roughness is provided in the next paragraph.) Figure 3 provides a photo of the PEEK model installed in the 20-Inch Mach 6 Tunnel, including an inset photo that zooms in on the roughness patch etched on one LE. The intent was to investigate distributed surface roughness on the order of the phosphor coating, so this model was an ideal test for this alternate approach for aerothermal data. Due to this added step of including distributed sand grain roughness near the LE, this model took much longer to build. An outside vendor was used to laser-etch the sand grain roughness into the PEEK material, which was part of the

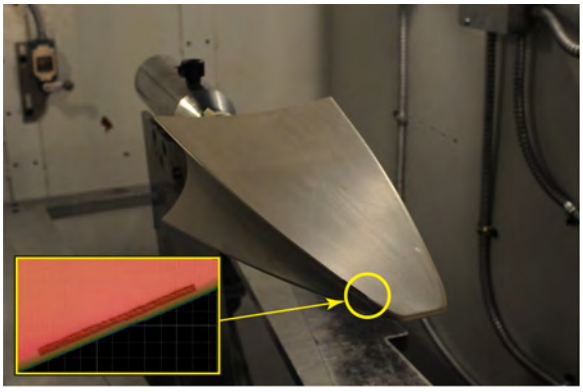

Figure 3. Third-scale BOLT PEEK model shown in tunnel: inset provides a closeup of LE with "phosphor" roughness laser etched onto surface.

* *The only difference between the preliminary and final geometries was a minor revision within the gutters.*

learning curve for this study (for a variety of reasons). This model took nearly a year to complete, but much of the delay was getting the outside vendor on contract, which was further slowed due to a government shutdown. As a rough estimate of a general build time using this approach (without the extraneous delays), it is probably closer to four months (two months to build the basic geometry using inhouse milling machines and 2 months to laser etch the roughness, depending on the vendor's workload). From a practicality perspective, it is definitely faster and cheaper to use the standard phosphor thermography approach, but only if minute and well-controlled surface details are not required. A third entry into LAL was completed with the JHU/APL built, highly-instrumented model (Ref 2), which was also a third-scale model. This model was a hybrid, half of which was built using PEEK and the other half using stainless steel with discrete sensors. Measurements on the JHU/APL model included unsteady pressures (PCB & Kulite), mean heat-flux (Schmidt-Boelter), and IR thermography on the PEEK.

The goal of the LaRC PEEK model was to investigate the effect of distributed surface roughness along the swept LE, with each one having a different level of roughness. On one side, there was a pristine LE (no roughness), while the other LE was laser-etched to replicate scans of the phosphor coating. This was done to investigate how much influence the surface roughness associated with our standard heating technique might have on boundary layer transition (BLT) through direct comparisons of the two sides. The opposite side of the model had even greater surface roughness added on each LE. Since the as-built condition of the roughness patches on each corner is still being assessed, the full set of results will be reported in another paper. Only the qualitative comparisons of the two leading edges (smooth vs. phosphors) are included here.

D. Test Conditions

The LaRC 20-Inch Mach 6 Air Tunnel (20M6) provides a freestream unit Reynolds number (*Re*) variation of 0.5 to 8.0 million per foot. For the half-scale model where the reference length is 17-in, the length Reynolds number (Re_L) is roughly 0.7 to 11.3 million, while for the third-scale model, the Re_L range is 0.5 to 8.0 million. As discussed in Ref. 1, the Re_L expected in flight for BOLT during the test window of interest varies from 1 to 20 million, largely covered by the available range within the 20M6. Also, the flight vehicle will be uncontrolled, but spin-stabilized at less than 5-Hz, relying upon the vehicle's static margin to maintain aerodynamic stability. Assuming a successful exoatmospheric reorientation maneuver, BOLT should reenter at the nominal angle of attack near zero. However, combined angle of attack and yaw excursions are likely, with less than ±2-deg being the desired goal but ±5-deg being acceptable. The wind tunnel test matrices were set up to explore the impact of these excursions, in both pitch and yaw, on the measured BLT results, in order to assist in establishing instrumentation needs and layout for flight.

E. Data Reduction & Uncertainties

For the phosphor thermography technique, heating rates were calculated using IHEAT, which is discussed in greater detail in Ref. 14. Additional details about the heat-transfer equations that are used to compute global heat-transfer results from global surface temperature measurements, using one-dimensional semi-infinite solid assumptions, are provided in Refs. 4 and 6. Heating distributions are presented in terms of the ratio of heat-transfer coefficients h/h_{FR}, where h_{FR} corresponds to the Fay and Riddell[15] stagnation-point heating to the leading edge radius. Reference 4 also provides a discussion on measurement uncertainty, indicating that the phosphor system measurement error is typically less than ±10% for windward surface data. However, the uncertainty is ultimately a function of the surface temperature rise during the run, so for cases with only a slight temperature increase (i.e., low heating), the uncertainties are higher and results are noisier. In Ref. 4, the overall experimental uncertainty of the windward data is quoted as approximately ±15% for an ideal high-heating case, with repeatability of the centerline heat transfer distributions found to be better than ±4%. For the present case, with lower windward heating typical of slender vehicles (e.g., BOLT) with low-angle compression (or even flow expansions), significantly higher uncertainties are expected and can be seen by higher amount of noise (or scatter) in the heating results.

For the IR thermography technique using PEEK as a model substrate, heat transfer calculations presented herein were completed with an exploratory code called QQHeat, which uses the same set of heat transfer equations as IHEAT. QQHeat was developed previously, in support of the Shuttle program (see Ref. 16), specifically for use with IR data. For this initial assessment, the use of QQHeat is preferred, as the existing IHEAT package has not been modified yet to work with the IR output files. Also, the PEEK thermal properties are still preliminary and will be updated based on findings from various testing labs before a final set is included in IHEAT. The properties that have been gathered thus far are consistent with the room temperature values that have already been reported in the literature.[13] However, because of the potential for significantly higher surface temperatures on models in the LAL, thermal properties are required over a wider range of temperatures than have been, thus far, reported. For the sake of the present paper, the

phosphor thermography results (and computational results, to be discussed in the next section) will be used as a benchmark for comparison to the newer PEEK/IR approach, as a way to check the current PEEK thermal properties.

IV. Computational Method

The Langley Aerothermodynamic Upwind Relaxation Algorithm (LAURA[17]) was used to compute the results presented herein. LAURA is a finite-volume, shock-capturing, structured-grid, computational fluid dynamics (CFD) tool specialized for hypersonic reentry flows. Either the Euler, thin-layer Navier-Stokes, or full Navier-Stokes equations are relaxed in pseudo time to a steady state. First-order inviscid fluxes are constructed using Roe's flux difference splitting with Harten's entropy fix and are extended to second-order using Yee's Symmetric Total Variational Diminishing (STVD) limiting. Second-order central differences approximate the viscous fluxes. LAURA can utilize point- or line-implicit relaxation and employs MPI to run efficiently on massively parallel computer architectures. LAURA has been validated for a range of flow conditions and vehicle shapes, including the Space Shuttle Orbiter[18], blunt planetary configurations[19], and slender lifting bodies[20].

Solutions were computed with laminar full Navier-Stokes on a computational mesh containing approximately 25 million cells (medium mesh) covering a quarter of the BOLT vehicle. Figure 4 compares centerline heating results of a basic grid refinement study using three grid levels, with coarser grids constructed by removing every other surface point. The finest mesh consisted of 491 blocks with 33 x 33 x 201 points per block. The 201 points through the layer remained unchanged for all levels of mesh refinement. The left axis in Fig. 4 indicates the nondimensional heating levels, h/h_{FR}. Three computed heating results are shown for each level of refinement (coarse, medium, and fine), along with the heating value based on Richardson's Extrapolation[21]. Richardson's method provides a representation of a spatially converged (h --> 0.0) solution and in this work Richardson's distribution is based on coarse and medium mesh data. Computed fine mesh heating values were found to be in agreement with Richardson, indicating the fine mesh can be considered spatially resolved. Note, if flow physics are not accurately captured, there is no guarantee a spatially resolved mesh will provide accurate values.

The grid convergence index (GCI[22]), as defined by Roache (Eq.1), provides an estimate of discretization error. The subscripts 2 and 3 represent the medium and coarse levels, respectively, r is the spacing ratio, p is the order of the scheme, and f is the quantity of interest. The following constants were used for this work: r and p were two (2) and the factor of safety (Fs) was 1.25.

$$GCI = 100.0 * Fs * \frac{\left|\frac{f_2 - f_3}{f_2}\right|}{(r^p - 1)} \quad (1)$$

The right axis of Fig. 4 presents the GCI, which indicates the percent error in heating between the medium mesh and a spatially converged answer. The GCI varies from nearly zero along the first half of the vehicle and increases to 13% over the latter half. While 13% is not an insignificant percentage, the absolute change in heating toward the trailing end of centerline is quite small. The heating sensitivity to mesh refinement over the latter half is believed to be due to boundary layer build-up on centerline.

The angle of attack was zero for all cases, hence the use of the quarter-body geometry. Each grid is solution adapted for bow shock alignment and boundary layer clustering using the shock adaption algorithm in LAURA, this effectively distributes off-body points to provide credible heat transfer. Along each line normal to the surface, this algorithm redistributes points such that a limited number (i.e., 5) remain in the freestream and the cell height spacing at the wall is based on a user-prescribed wall cell Reynolds number (0.50). Having a machine zero L2 error norm or a percentage change in heating of less than 0.1% over 5000 iterations defined convergence.

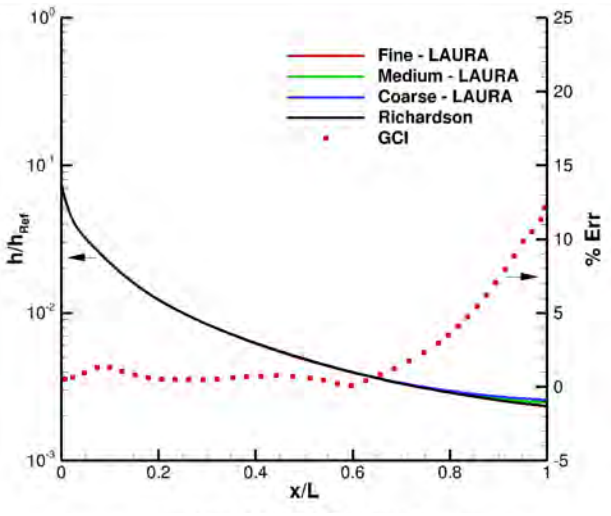

Figure 4. Mesh refinement: nondimensional heating and grid convergence index along model centerline for nominal alpha and beta.

V. Results & Discussion

Multiple test entries into the LAL 20-Inch Mach 6 Air Tunnel in support of BOLT will be discussed in the following subsections. First, the phosphor thermography results that were obtained prior to project kick-off are provided, with discussion of trends and observations. Then, some IR results are presented, primarily to compare and contrast the two test techniques. Only a small subset of the IR results are to be included here. Next, an overview of the test that was conducted at JHU/APL's request is included, but the actual test results are intended to be reported in a separate JHU/APL report. Finally, plans for a final test entry, to investigate heating from the BOLT vehicle to the payload adaptor for the launch stack, will be briefly discussed.

A. Preliminary Transition Assessment – Test 7027

Figure 5 provides global heat transfer images for a range of model length Reynolds numbers (Re_L) for BOLT at a nominal angle of attack (α=0 deg) and sideslip (β=0 deg). This Re_L sweep is sufficient to reveal the systematic movement of transition, indicated by BLT onset fronts seen as two higher-heating lobes, symmetric on either side of the model centerline (CL). At the lowest Re_L, Fig. 5(a), the lobes are just appearing near the back end of the model, while at the highest Re_L, Fig. 5(d), the lobes have moved forward to be closer to the nose and nearly along the swept leading edges. The central region (along the model CL) appears resistant to transition, while the outboard sections (nearer the swept LE) are much more sensitive to increasing Reynolds number. As reported in Ref. 2 from observations gleaned from supporting CFD, the central region is characterized by a thick boundary layer due in part to inflow coming from the swept LE. This central region does not appear "well-modeled by most instability codes"[2] and therefore, will be considered a challenging region for the BOLT team to understand. The outer regions, on the other hand, are more traditional, with a thinner boundary layer. Instability calculations suggest that both second mode and crossflow instabilities are amplified in this outer region.

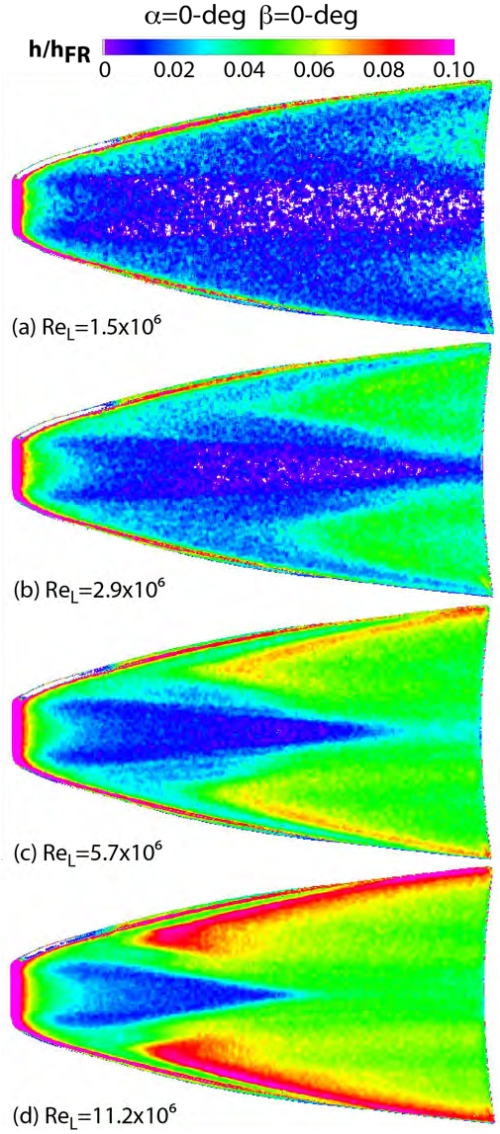

Figure 5. Effect of Reynolds number at nominal alpha (0 deg) and beta (0 deg).

Reference 2 also includes experimental IR and temperature sensitive paint (TSP) results from Purdue's Mach 6 Quiet Tunnel, showing BLT patterns for both noisy and quiet flow. In the quiet results, only vortices are observed as BLT onset does not occur even at the highest Re condition available. However, for the noisy results, BLT onset fronts are seen that are similar to what is shown here (two lobes on either side of CL).

Since the outboard regions are Reynolds number sensitive, it is quite likely that instability mechanisms are contributing to the observed results. There are even hints of streaks just ahead of the transition fronts, which provides further connectivity to the quiet tunnel results and instability calculations of Ref. 2.

Figure 6 provides the global heat transfer images for a range of angles-of-attack from α=±5 deg for fixed Re_L=5.7x10^6 and β=0 deg. From a trend perspective, increasing α for a fixed Re_L results in the symmetric BLT lobes progressing slowly toward the nose. However, the relative impact of α appears somewhat less than the influence of Re_L. For instance, the transition front at α=5 deg, Fig. 6e, is not nearly as far forward as the highest Re_L at α=0 deg case, Fig. 5d. A doubling of Re_L (compare 5c to 5d) has more influence on the transition

fronts than an increase in angle of attack of two-and-a-half times (compare against 6d & 6e). For negative angles of attack (resulting in the measurement surface being on the leeside), the transition front appears largely stationary. Although, for the case of -5 deg (Fig. 6a), pronounced streaks emanate from the outboard region of the 2D nose section, perhaps an indication of a different BLT mechanism becoming important. As noted in Ref. 2, α effects for BOLT do not strongly affect the patterns much under quiet conditions: "The results are quite similar at each angle, though the number of crossflow streaks and the specific path vary slightly."

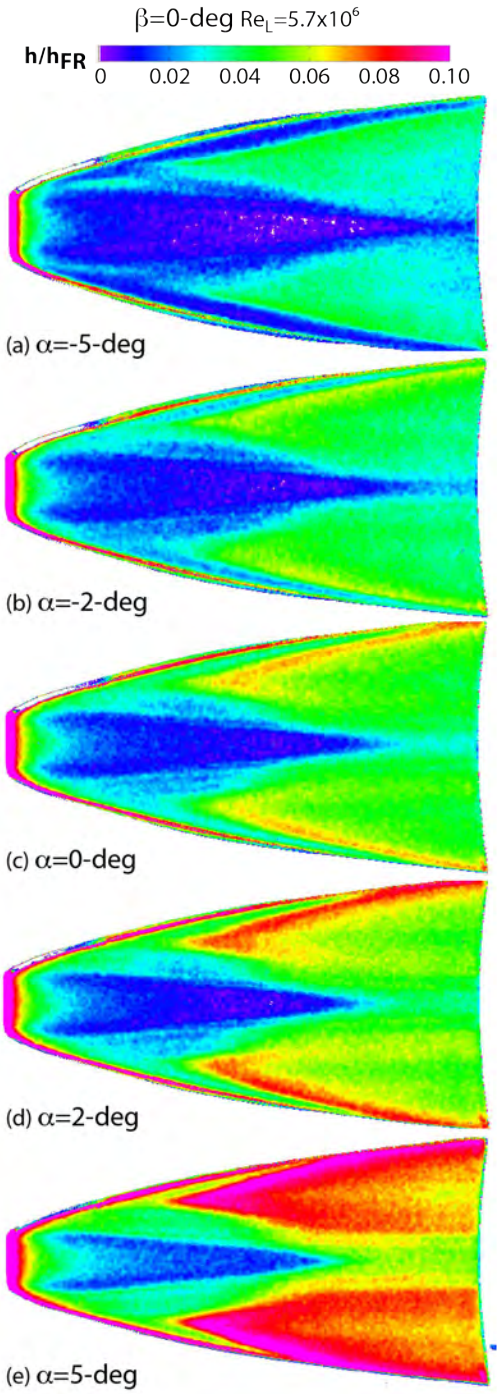

Figure 6. Effect of angle of attack for nominal beta (0 deg) and Re_L=5.7x10^6.

Figure 7 provides the global heat transfer images for a range of sideslip angles from β=0 deg to 5 deg for α=0 deg and Re=5.7x10^6. Due to symmetry, only results from sideslip in one direction are shown. In comparison to the nominal β=0 deg case, there is no significant change in the relative sizes of the two lobes for β=2 deg (Fig. 7b). But for β=5 deg (Fig. 7c), the resulting BLT onset fronts are very asymmetric, with the side toward the flow becoming slightly larger and the side away becoming significantly smaller. In reference to the central (low heating) region, 2-deg sideslip resulted in a shift away from the CL of less than a quarter of the span, while the shift was almost half the span away from the CL for 5-deg sideslip.

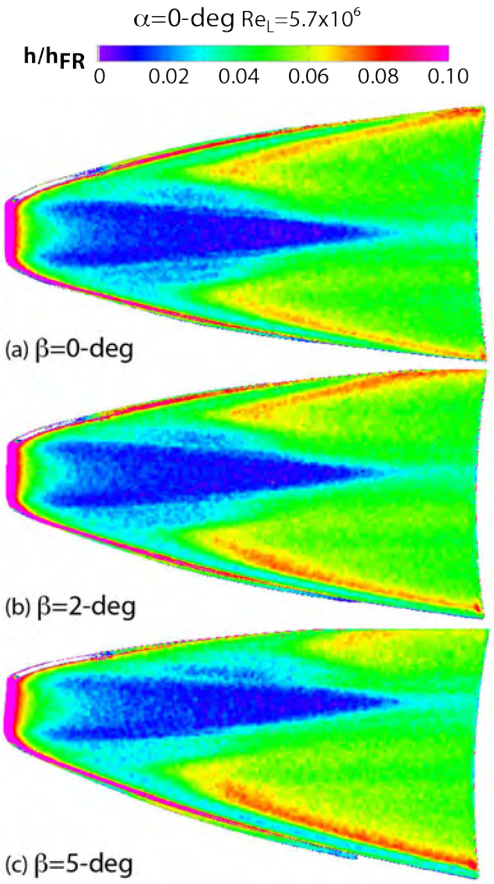

Figure 7. Effect of sideslip at nominal alpha (0 deg) and Re_L=5.7x10^6.

Reference 2 notes: "It is clearly evident that the BOLT geometry is much more sensitive to sideslip than angle of attack. The streak paths are shifted dramatically at 4-deg β." Understanding this sensitivity will become especially important for design of the instrumentation layout for the flight vehicle.

Sample combinations of off-nominal α and β on the global heat transfer results are provided in Figure 8. While other combinations were obtained, only a few of the most interesting cases are included here. As one might expect, extreme combinations of α and β result in very asymmetric heating patterns (see Fig. 8c). Unfortunately, for a spin-stabilized sounding rocket, the actual α and β at the time of interest with post-flight data analysis will not be known *a priori*. These extreme cases with combined α/β effects are intended to provide guidance for determining whether any post-flight wind-tunnel entries might be required for comparison against the flight data.

Figure 9 provides the global heat transfer images for the BOLT gutter region for a range of Re_L at nominal α and β (0 deg). Results in the gutter were obtained for other α and β (and combinations), which were presented to the BOLT project at kickoff, but are not included here. This is the only test entry conducted to date for the BOLT project that includes data from the gutter region. It is interesting to note that the BLT patterns in the gutter at the highest Re_L look qualitatively similar to the results on the main surface (symmetric lobe fronts nearly ¾ the way up the forebody with a central laminar region) except that the image looks compressed. While the gutter region is not a focus for BOLT, there are plans to at least partially instrument the gutters for flight.

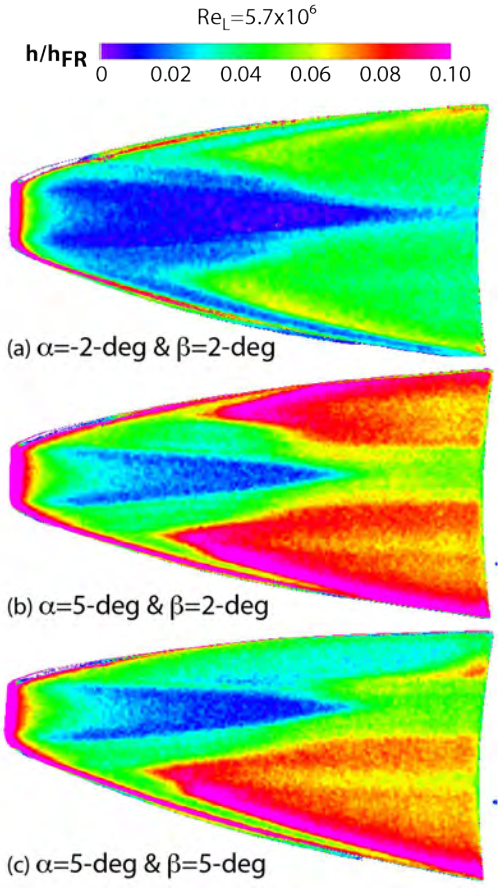

Figure 8. Comparison of results for various angles of attack and sideslip at Re_L=5.7x10^6.

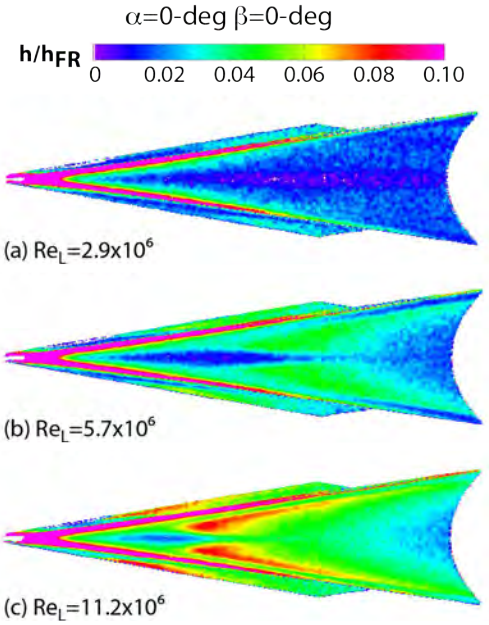

Figure 9. Effect of Reynolds number on the side gutter at nominal alpha (0cdeg) and beta (0 deg).

B. Leading Edge Roughness Study – Test 7031

Figure 10 provides global heat transfer results, computed with QQHeat, with the leading edge roughness PEEK model for a range of Re_L at nominal α and β. These results are qualitatively similar to the results shown earlier, with the same two-lobed transition fronts and movement, although the actual Re_L is smaller here due to the shorter model length. Note that the images are less noisy than the phosphor results, especially in the lower heating central region, thus providing better clarity of the streaks. Also, note that the IR imager picks up a signal from everything in its view, including the injection plate below the model. This is in contrast to the phosphor thermography approach, where only the model fluoresces and is therefore seen by the camera. Thus, the cropped IR-produced images shown in Fig. 10 include the background, pending a method to strip out all but the model. The intention is to eventually integrate the IR analysis within a future version of IHEAT. Removal of

the superfluous signal would be included in that process, to allow easier definition of the model for doing line cuts and/or mapping results to a 3D geometry.

As mentioned previously, the model built for this study had different levels of distributed surface roughness built directly into the PEEK along three of four swept leading edges. The results shown here are for Side A of the model, where one LE had no roughness added (the lower LE in each image) and the other replicated the phosphor coating (the upper LE). The symmetry (upper side to lower) suggests that the surface roughness associated with phosphor coatings is not significant enough to alter the BLT transition front patterns. This is good, but not unexpected, news for the phosphor technique.

Figure 11 provides a comparison of extracted centerline data from both the phosphor (Test 7027) and IR (Test 7031) studies to CFD for the range of Re_L at nominal α and β. The phosphor results (shown with no symbols) are easily identifiable by the "noise," with scatter on either side of the CFD results (plotted with circle symbols) for laminar conditions. This is a fairly typical comparison of the phosphor results to CFD, showing that this well characterized test technique compares favorably against predictions. However, due to the low heating condition, the phosphor scatter is quite high. Shown in the plot, for reference, is an error bar on the computations of ±50%. The phosphor scatter is on that order. The PEEK/IR results, on the other hand, are biased to the high side of the phosphor results, and fall just within the 50% mark in reference to the CFD. This provides a clear indication that the PEEK thermal properties need further assessment and refinement. Two more independent checks of thermal properties for PEEK are currently underway. While further work is

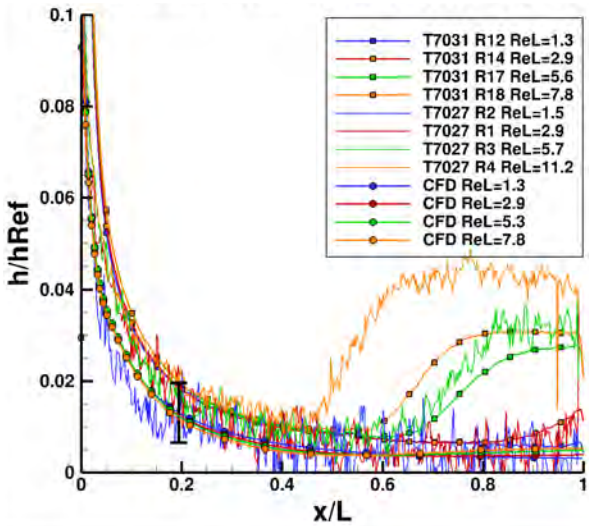

Figure 11. Comparison of centerline heating data from T7027, T7031, and CFD.

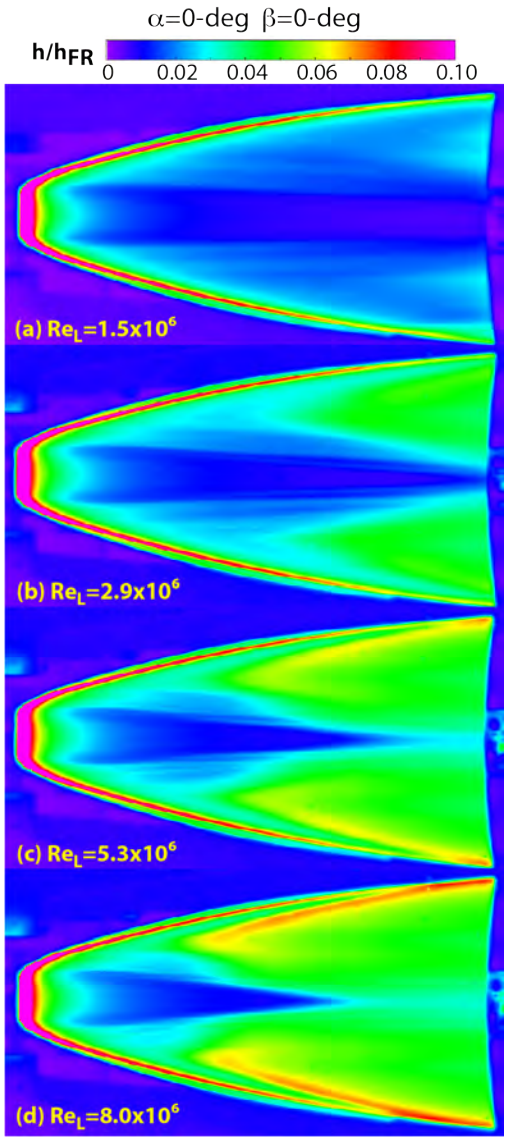

Figure 10. Effect of Reynolds number at nominal alpha (0 deg) and beta (0 deg).

required with the IR thermography approach, with PEEK as the model substrate, to advance it to quantitative status, two things stand out as positives attributes: (1) the lack of noise in the results, even for a case such as this, with low heating, and (2) the consistent results for identifying transition onset. Note that, even with two different scale models, BLT onset was nearly identical between the two techniques, occurring at x/L=0.65 for the cases near Re_L=5.7x10^6 (both with green lines).

C. JHU/APL-Directed Study – Test 7032

The very next 20M6 tunnel entry was also in support of BOLT, using the JHU/APL model (see Ref. 2) that was making the rounds through various national facilities. Specifically, the goals of this entry were to measure

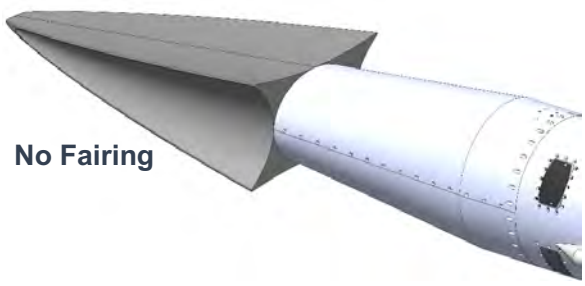

Figure 12. View of the notional attachment of BOLT to the payload section without a fairing.

boundary-layer instabilities and the effects of steps on BLT at Mach 6 on the JHU/APL subscale BOLT model. The matrix was set up at JHU/APL's request, with a majority of the runs dedicated to looking at steps at different locations and heights for a small range of conditions (nominal and ±2-deg of α and β). These step cases were primarily focused on joint tolerances for flight. The locations for steps on the model were selected to coincide with the joints in the current flight design between the nose, stainless steel, and aluminum sections. Measurements included unsteady pressures (PCB and Kulite), mean heat flux (Schmidt-Boelter) and IR thermography on the PEEK section. The test was successfully completed this past summer and the results were provided to JHU/APL, some of which are captured within Refs. 23 and 24.

D. Launch Fairing and Discrete Roughness Studies (In Preparation)

One final test entry is planned, specifically to look at aeroheating environments on fairing designs that are presently being considered for the payload section downstream of the flight geometry. The entire launch stack consists of the flight geometry, the payload system, and the launch vehicle system (as shown in Fig. 2 of Ref. 1). The flight geometry, as mentioned previously, is being designed and built by JHU/APL, which includes the instrumentation package, sensor collection boards, and wiring. The payload system will be provided by the Air Force Research Laboratory Aerospace Systems Directorate (AFRL/RQ) in Dayton OH, and includes systems to support data acquisition, telemetry, and GPS. The launch vehicle, provided by DLR Moraba, consists of a two-stage sounding rocket stack (Improved Orion and S-31), including an exoatmospheric reorientation system. The interface between the flight geometry and the payload section (shown in Fig. 12) is presently a concern and focus of the team. Preliminary analysis of the aerodynamics of the launch stack suggests that a fairing in this region, to reduce flow separations and reattachments on the payload section (and possible aero-buffeting), would improve controllability across the trajectory. Computational studies with various fairings are underway. LaRC is planning to test several fairing designs, along with a no-fairing case, in order to compare and contrast reattachment heating on the payload section.

VI. Concluding Remarks

An overview of support by LaRC to the BOLT flight project has been discussed, ranging from an early phosphor thermography wind tunnel study on a half-scale model to more recent IR thermography studies on third-scale models to an upcoming assessment of heating on the payload section with and without fairings. The phosphor thermography results are presented in detail, including trends and observations from the data. The results from the newer IR approach are compared against results from both phosphors and CFD in order to assess the fidelity of the thermal properties of the model substrate, PEEK. A key finding from the present analysis is that further refinement of the PEEK thermal properties is required in order to drive this newer technique to quantitative status.

The most significant trend was the observation of a two-lobed transition pattern, symmetric on either side of the centerline, that was strongly influenced by an increase in Reynolds number. This two-lobed pattern appeared rather insensitive to model angle of attack, over the range of interest (±5-deg). Sideslip, on the other hand, more strongly affected the symmetry of the patterns for the same range. Flight instrumentation should be placed with consideration of this sideslip sensitivity. The trends noted here are consistent with those listed in other BOLT papers.

In reference to the new IR thermography approach, some pros and cons have been identified. On the issue of practicality, the use of PEEK as the substrate material resulted in models that were slightly more expensive than our conventional phosphor thermography approach, but, more importantly, took much longer to build. And, while the material appears robust enough for the present entry into the 20-Inch Mach 6 tunnel (no obvious surface degradation), the true test will be when its tested in the 31-inch Mach 10 tunnel (which has a much higher temperature potential). On the quantitative side, the material does offer good optical properties, with its high surface emissivity, but there are concerns that the material is also highly reflective to thermal radiation (not shown here, but seen in other tests). And while the thermal properties still need refinement, the technique does offer better sensitivity for lower temperatures. All in all, the new IR thermography approach does show promise, but it is not likely to replace our phosphor thermography technique for most situations.

Acknowledgments

Funding for LaRC's contributions to the BOLT project has been provided by the Hypersonics Technology Project. The authors would also like to thank Chase Litzner and Richard Wheless for assistance with model design, Rob Andrews, Mike Powers, LaRC's Fab shop, and the EDM Dept (of Bartlett, IL) for help with building models, the 20M6 Tunnel support staff, Carey Scott, Paul Larsen, and several visiting interns from JHU/APL for assistance during tunnel testing.

References

1 Wheaton, B. M., Berridge, D. C., Wolf, T. D., Stevens, R. T., and McGrath, B. E., "Boundary Layer Transition (BOLT) Flight Experiment Overview," AIAA Paper 2018-2892, Jun 2018.

2 Berridge, D. C., McKiernan, G. R., Wheaton, B. M., Wolf, T. D., and Schneider, S. P., "Hypersonic Ground Tests In Support of the Boundary Layer Transition (BOLT) Flight Experiment," AIAA Paper 2018-2893, Jun 2018.

3 Berger, K., Rufer, S., Hollingsworth, K., and Wright, S., "NASA Langley Aerothermodynamic Laboratory: Hypersonic Testing Capabilities," AIAA Paper 2015-1337, Jan. 2015.

4 Merski, N R., "Global Aeroheating Wind-Tunnel Measurements Using Improved Two-Color Phosphor Thermography Model.", Journal of Spacecraft and Rockets, Vol. 36, 2, 1998, pp. 160-170.

5 Buck, G. M., "Automated Thermal Mapping Techniques Using Chromatic Image Analysis," NASA TM 101554, April 1989.

6 Buck, G. M., "Surface Temperature/Heat Transfer Measurement Using A Quantitative Phosphor Thermography System," AIAA Paper 91-0064, Jan. 1991.

7 Berry, S. A., Bouslog, S. A., Brauckmann, G. J., and Caram, J. M., "Shuttle Orbiter Experimental Boundary-Layer Transition Results with Isolated Roughness," Journal of Spacecraft and Rockets, Vol. 35, No. 3, 1998, pp. 241-248.

8 Berry, S. A., Horvath, T. J., Hollis, B. R., Thompson, R. A., and Hamilton, H. H., "X-33 Hypersonic Boundary Layer Transition," Journal of Spacecraft and Rockets, Vol. 38, No. 5, 2001, pp. 646-657 (see also AIAA Paper 99-3560, June 1999).

9 Horvath, T. J., Berry, S. A., Merski, N. R., Fitzgerald, S. M., "X-38 Experimental Aerothermodynamics," AIAA Paper 2000-2685, June 2000.

10 Micol, J. R., "Aerothermodynamic Measurement and Prediction for a Modified Orbiter at Mach 6 and 10 in Air," Journal of Spacecraft and Rockets, Vol. 32, No. 5, 1995, pp. 737-748.

11 Hollis, B. R., Horvath, T. J., Berry, S. A., Hamilton, H. H., and Alter S. A., "X-33 Computational Aeroheating Predictions and Comparisons with Experimental Data," Journal of Spacecraft and Rockets, Vol. 38, No. 5, 2001, pp. 658-669 (see also AIAA Paper 99-3559, June 1999).

12 Loomis, M. P., Venkatapathy, E., Davies, C. B., Campbell, C. H., Berry, S. A., Horvath, T. J., and Merski, N. R., "Aerothermal CFD Validation and Prediction for the X-38 Program," AIAA Paper 97-2484, June 1997.

13 Borg, M. P., and Kimmel, R. L., "Simultaneous Infrared and Pressure Measurements of Crossflow Instability Modes for HIFiRE-5," AIAA Paper 2016-0354, Jan. 2016.

14 Mason, M. L., and Rufer, S. J., "Features of the Upgraded Imaging for Hypersonic Experimental Aeroheating Teasting (IHEAT) Software," AIAA Paper-2016-4322, Jun 2016.

15 Fay, J. A., and Ridell, F. R., "Theory of Stagnation Point Heat Transfer in Dissociated Air," Journal of Aeronautical Sciences, Vol. 25, No. 2, 1958.

16 Horvath, T. J., "Experimental Aerothermodynamics in Support of the Columbia Accident Investigation," AIAA Paper 2004-1387, Jan. 2004.

17 Mazaheri, A., Gnoffo, P.A., Johnston, C.O., Kleb, W.,"LAURA User's Manual:5.5-65135," NASA TM-2013-217800, Feb 2013.

18 Gnoffo, P.A., Weilmuenster, K.J., "Multiblock Analysis for Shuttle Orbiter Re-Entry Heating from Mach 24 to Mach 12," AIAA Paper 93-2813, July 1993.

19 Gnoffo, P.A., Braun, R. D., Weilmuenster, K.J., Mitcheltree, R.A., Engelund, W.C., Powell, R.W., "Prediction and Validation of Mars Pathfinder Hypersonic Aerodynamic Database," Journal of Spacecraft and Rockets, Vol. 36, No. 3, 1999, pp. 367-373.

20 Thompson, R.A., Gnoffo, P.A., "Application of the LAURA Code for Slender Vehicle Aerothermodynamics," Journal of Spacecraft and Rockets, Vol. 29, No. 1, 1992, pp. 16-23.

21 Richardson, L.F., "The Deferred Approach to the Limit," Transactions of the Royal Society of London, Series A, Vol. 226, 1927, pp. 229-361.

22 Roache, P.J., "Perspective: A Method for Uniform Reporting of Grid Refinement Studies," ASME Journal of Fluids Engineering, Vol. 116, No. 3, 1994, pp. 405-413.

23 Berridge, D.C., Kostak, H.E., McKiernan, G.R., Wheaton, B.M., Wolf, T.D., and Schneider, S.P., "Hypersonic Ground Tests With High-Frequency Instrumentation In Support of the Boundary Layer Transition (BOLT) Flight Experiment," pending paper for AIAA SciTech 2019.

24 Kostak, H.E., Bowersox, R.D.W., McKiernan, G.R., Thome, J., Candler, G.V., King, R.A., "Freestream Disturbance Effects on Boundary Layer Instability and Transition on the AFOSR BOLT Geometry," pending paper for AIAA SciTech 2019.